Journal of Artificial Intelligence and Data Mining (JAIDM), Vol. 14, No. 2, 2026, 221-233.

Shahrood University of Technology

Journal of Artificial Intelligence and Data Mining (JAIDM)
Journal homepage: http://jad.shahroodut.ac.ir

Research paper

Low-light Image Enhancement Based on Retinex Theory Using the Evolutionary PSO Algorithm

Ali Shabani Badi[1], Kambiz Rahbar[1,*], Ziaeddin Beheshtifard[1] and Maryam Khademi[2]

1. Department of Computer Engineering, ST.C., Islamic Azad University, Tehran, Iran,
2. Department of Applied Mathematics, ST.C., Islamic Azad University, Tehran, Iran,

Article Info

Article History:
Received 01 June 2025
Revised 15 August 2025
Accepted 14 October 2025

DOI:10.22044/jadm.2025.16339.2755

Keywords:
Low-light Image Enhancement, PSO Evolutionary Algorithm, Retinex Theory, Gamma Correction.

**Corresponding author: kambiz.rahbar@iau.ac.ir (K, Rahbar).*

Abstract

This paper introduces a novel approach to enhance the quality of images captured under low-light conditions. The method optimizes the parameters of the established Li method by employing the evolutionary Particle Swarm Optimization (PSO) algorithm. A key contribution of this research is the formulation of a comprehensive loss function for the PSO algorithm, derived from the integration of entropy loss, edge pixel loss, and average desired image brightness loss. The objective of this optimization process is to determine the optimal parameter set for the base method, thereby improving the preservation of image structure, increasing brightness while maintaining edge details, and ensuring the overall brightness of the resulting image remains within a desirable range. The entropy loss function increases the details of the image, which leads to an enhancement in the image contrast. The edge loss function enhances the edges of the image. The increase in edge pixels strengthens and sharpens the boundary lines of objects present in the image, which consequently improves the image clarity. The brightness loss function adjusts the image brightness toward an optimal state. The average brightness of the image pixels approaches a value of 0.6 (within the range of zero to one), which helps normalize and optimize the image brightness. An iterative optimization strategy is employed to address the resulting optimization problem. The performance of the proposed method is evaluated through quantitative and qualitative analyses on the SICE dataset and benchmarked against several state-of-the-art low-light image enhancement techniques. Quantitative evaluation, utilizing metrics such as PSNR, SSIM, PIQE, NIQE, BRISQUE, and NIMA, demonstrates that the proposed parameter tuning of the base method, guided by the PSO algorithm and our comprehensive loss function, achieves competitive or superior performance in preserving image structure and details, generating images with natural visual quality, and suppressing noise in comparison to numerous existing methods. This research highlights the efficacy of the evolutionary PSO algorithm in identifying optimal configurations for a physical model-based method aimed at enhancing the quality of low-light imagery.

1. Introduction

Images captured under low-light conditions often suffer from issues such as poor visibility, low contrast, and significant noise. The degraded quality of these images can substantially reduce the performance of computer vision algorithms, highlighting the importance of image brightness

enhancement techniques in such scenarios. These techniques can be broadly classified into histogram-based, deep learning-based, and Retinex-based approaches. The first category employs histogram manipulation to improve image quality. However, direct brightness enhancement and methods based on histogram equalization (HE) [1] can lead to undesirable effects such as saturation and noise amplification. Some researchers have drawn parallels between inverted low-light images and hazy images, applying dehazing techniques [2], including BM3D-based methods [3], which were initially developed for post-enhancement noise reduction. Nevertheless, the underlying physical principles of these methods are not always well-defined, and the sequential order of enhancement and noise removal presents a challenge.

In the second category, deep learning and neural networks are employed for image enhancement. Deep learning-based methods, such as LLNet [4], have been proposed for the simultaneous enhancement and denoising of low-light images; however, their performance can be constrained by the limitations of the training data. The LLFormer method [5] presents an unsupervised transformer-based learning model that utilizes a self-attention module and a fusion block to enhance image quality. Zero-DCE [6] is another widely adopted method for low-light image enhancement. Nevertheless, its efficacy depends on the availability of training data encompassing diverse exposure levels, and it may struggle to effectively process images with uneven illumination, extremely low illumination, or overexposure. To address this limitation, the Zero-DiDCE method [7] was introduced. This model offers a dual-illumination deep curve estimation approach that does not require reference images, enabling adjustment of image brightness levels. It also incorporates an adaptive curve to manage images with varying luminances and a brightness control mechanism. Furthermore, the method described in [8] proposes an unsupervised learning model that uses a deep neural network to estimate a pixel-level curve for adjusting the dynamic range of an image, again without the need for reference images.

In the third category, Retinex theory [9] posits that images can be decomposed into reflectance and luminance components. Various methods based on this theory have been developed, including single-scale Retinex [10] and multi-scale Retinex [11], as well as approaches utilizing bright-pass filters [12,13] and light map refinement [14]. However, a common drawback of these methods is their tendency to amplify significant noise present in the original image. In [15], it is argued that the logarithmic transformation inherent in traditional Retinex models is not well-suited for handling noise effectively. To address these limitations, R2RNet [16] presents a Retinex-based model designed for low-light image enhancement. This model comprises three sub-networks: Decom-Net (for image decomposition), Denoise-Net (for noise reduction), and Relight-Net (for contrast enhancement and detail preservation). Notably, R2RNet leverages both spatial and frequency information from the image to not only improve contrast but also to preserve fine details.

The Li method [17] builds upon a robust Retinex model that incorporates a noise term. The classical Retinex model decomposes an image into two fundamental components: reflectance (R), representing the intrinsic surface properties, and luminance (L), representing the scene illumination. Traditional Retinex approaches often employ logarithmic transformations [18] to simplify calculations and modeling. However, this transformation presents challenges when dealing with low-light images, which inherently contain significant noise. Beyond the Retinex model, image decomposition methods [19,20-22,23] have also been utilized for estimating reflectance and luminance. These methods typically rely on the assumption that light sources are distant and that the scene is not influenced by multiple colored light sources. These assumptions often break down in low-light scenarios, which can involve strong, proximal light sources.

Given the presence of substantial noise in low-light images, the classical Retinex model appears insufficient for enhancing these types of images. To address this, the Li method proposes a robust Retinex model, as shown in (1), which incorporates a noise term (N). This formulation shares similarities with intrinsic image decomposition models that consider factors such as luminance (L), reflectance (R), and specular reflections (C). While many studies [19,24,25] omit the specular reflection component for simplicity, this paper includes a noise term (N) in the model. Unlike specular reflections, noise is more uniformly distributed throughout the image.

$$I = R \circ L + N \tag{1}$$

$$\log(R) + \log(L) \neq \log(R \circ L + N) \tag{2}$$

According to (2), the inclusion of the noise term (N) challenges the suitability of employing logarithmic transformation within the Retinex model. More significantly, the presence of noise

(N) can substantially influence gradient variations in the logarithmic domain. Specifically, when the reflectance value (R) is small, as frequently occurs in dark and noisy regions, even minor fluctuations in R caused by noise can translate into significant changes in the gradient. This phenomenon can lead to noise amplification in the enhancement results, consequently degrading visual quality. Based on this analysis, the direct application of the logarithmically transformed Retinex model is ill-advised for enhancing low-light images.

In low-light image enhancement, it is crucial to account for the noise term (N). Neglecting this term leads to the noise present in the input image (I) being incorrectly incorporated into either the luminance (L) or reflectance (R) component. Given that many enhancement methods primarily focus on manipulating the luminance (L) component and derive reflectance as R = I/L, this inevitably results in noisy outputs. Consequently, a separate denoising step is often necessary after the enhancement process [14,15].

In the field of Retinex-based image enhancement, several pioneering works have implicitly or explicitly addressed the issue of noise. For instance, Old [26] proposed constraining the smoothness of luminance and reflectance using two bidirectional filters in the logarithmic transform domain. This model accounts for the proximity of the luminance to the observed image and assumes multiplicative noise. Similarly, methods proposed in [27] and [28] directly remove noise from the estimated reflectance. Li et al. [27] employed edge-preserving smoothing [29], while Yu et al. [28] utilized the guided filter [30] for this purpose. In contrast to these prior approaches, this paper aims to simultaneously improve the visibility of low-light images and mitigate the effects of noise. Specifically, the Particle Swarm Optimization (PSO) algorithm is used to optimize the Li method. The gamma parameter in the Li method is used to adjust the brightness of the enhanced image. We employ the PSO optimization algorithm to find the optimal gamma value. To achieve this, we define a three-part loss function to evaluate the gamma values generated by the PSO algorithm. This loss function comprises the sum of the entropy loss function, the number of edge pixels, and the desired average brightness. The details of the proposed method are presented in Section 2, the evaluation and comparison of methods are provided in Section 3, and the conclusion is given in Section 4.

2. Image Enhancement with the PSO Algorithm and Related Loss Functions

This section presents the proposed image enhancement method, which is based on Li's method and employs the evolutionary PSO algorithm for parameter optimization. The gamma parameter used in Li's method is treated as the population within the PSO algorithm. For each gamma parameter, an enhanced image is generated using Li's method. Subsequently, each enhanced image is evaluated using a three-part loss function. Finally, the gamma parameter yielding the optimal score is selected as the final gamma parameter. Figure 1 illustrates the steps involved in selecting the optimal gamma value for image enhancement. The following subsections detail the framework of Li's method and explain the optimization of the gamma parameter using the PSO algorithm, along with the associated loss functions.

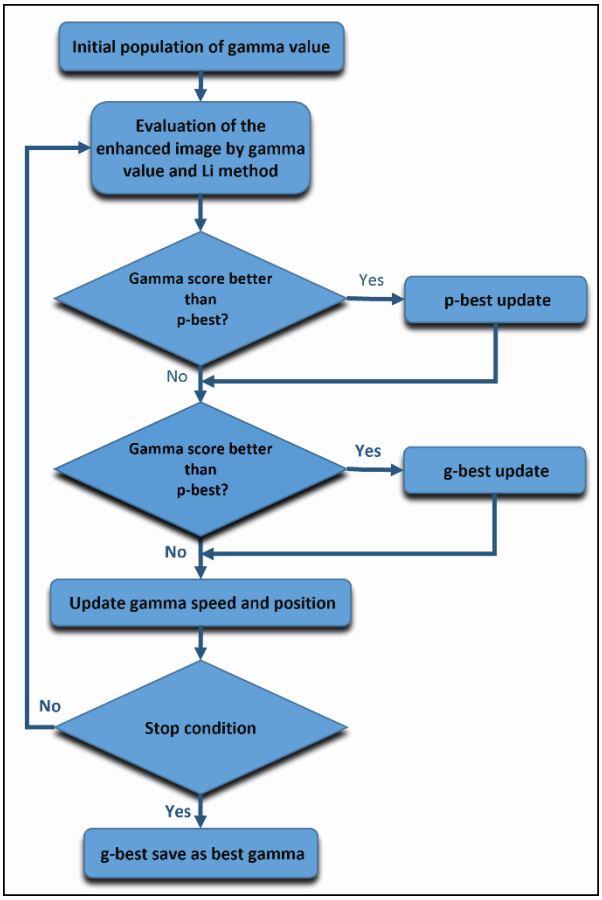

Figure 1. Steps of the PSO algorithm and selection of the best gamma value for image enhancement by Li's method.

2.1. Li's method explained

The Li method is applied to the V channel within the HSV color space. Given a low-luminance color image S as input, the method first transforms it into the HSV color space. The proposed decomposition is then applied to the normalized V channel image, denoted as I, to obtain the luminance (L) and reflectance (R) components. Subsequently, to

enhance darker regions, the luminance L is adjusted, generating the adjusted luminance $\hat{L}$. This adjusted luminance $\hat{L}$ is then combined with the reflectance component R to produce the enhanced V channel image $\hat{I}$. Finally, the enhanced HSV image is converted back to the RGB color space, yielding the final enhanced result $\hat{S}$.

2.1.1. Basis Analysis

In this subsection, a new decomposition model is introduced that simultaneously estimates the reflectance R and the luminance L of the input image I as follows:

$$\arg\min_{R,L} \|R \circ L - I\|_F^2 + \beta \|\nabla L\|_1 + \omega \|\nabla R - G\|_F^2 \quad (3)$$

Where β and ω are coefficients that control the importance of different terms. $\|.\|_1$ and $\|.\|_F$ denote the Frobenius norm and the ℓ_1 norm, respectively. In addition, ∇ is the first-order differential operator and G is the adjusted gradient of I, which will be discussed in (4). The role of each term in (3) is interpreted as follows:

$\|R \circ L - I\|_F^2$ It limits the relationship between the observed image I and the reconstructed image $R \circ L$.

$\|\nabla L\|_1$ It corresponds to minimizing the total variation and considering the piecewise smoothness of the illumination map L.

$\|\nabla R - G\|_F^2$ It minimizes the distance between the reflection gradients R and G (the adjusted version of the input gradient I), so that the structural information of the reflection is enhanced.

Previous works [31] have employed the ℓ_2 norm on brightness gradients and the ℓ_1 norm on reflectance gradients. However, it has been observed that the brightness distribution in most natural low-light images is non-uniform (i.e., they contain relatively bright regions). This suggests that using an ℓ_2 norm, which enforces smooth spatial illumination, is not appropriate for these images. Consequently, these methods often produce visible halo artifacts. This is because the ℓ_2 norm tends to create blurred boundaries around areas exhibiting significant brightness transitions, a common characteristic of low-light images. While the ℓ_1 norm is used to encourage piecewise smoothness of the reflectance, the decomposed reflectance remains influenced by low illumination. This is due to the data dependency term forcing the product of brightness and reflectance to approximate the halo-prone input image. In contrast, utilizing ℓ_1 smoothing to constrain brightness gradients helps preserve the overall structure of the images and yields improved visual quality.

As mentioned in the preceding section, low-light images are characterized not only by low visibility and high noise levels but also by low contrast. Given the inverse relationship between contrast and gradient values, this paper proposes manipulating the reflectance gradient values to enhance the contrast of the resulting image. To achieve this, a third term, $\|\nabla R - G\|_F^2$ is introduced into the objective function to constrain the dependence between ∇R and a guide matrix G. The matrix G is obtained by amplifying the gradient of the input image by a factor K. To balance the magnitude of G, the factor K is designed to adaptively apply fewer adjustments to areas with larger values and more adjustments to areas with smaller values. The formulation of G is given as follows [32]:

$$G = K \circ \nabla I \quad (4)$$

$$K = 1 + \lambda e^{-|\nabla I|/\sigma} \quad (5)$$

Specifically, ∇I is amplified by a factor K that is inversely related to the gradient magnitude. This amplification strategy results in smaller adjustments in regions with larger gradient magnitudes, while regions with smaller gradient magnitudes undergo greater amplification. Consequently, the adjusted gradient G tends toward a more uniform magnitude. Furthermore, λ controls the overall degree of amplification, and σ governs the rate of amplification across different gradient values. In Li's method, both parameters λ and σ are set to 10. For each input image, the matrix G needs to be calculated only once.

2.1.2. Alternative Analysis

As previously mentioned, the presence of noise in low-light images is unavoidable. Furthermore, the noise observed in natural images is often more complex than additive white Gaussian noise. Therefore, instead of estimating the noise distribution, this work aims to directly estimate a noise map from the input image. To explicitly estimate the noise map, the following optimization problem is also presented:

$$\arg\min_{R,L,N} \|R \circ L + N - I\|_F^2 + \beta \|\nabla L\|_1 + \omega \|\nabla R - G\|_F^2 + \delta \|N\|_F^2 \quad (6)$$

Where N represents the estimated noise map, and the term $\|N\|_F^2$ constrains the overall noise intensity. The dependency term involving the noise map is included to ensure the model's accuracy, meaning that the estimated brightness, reflectance,

and noise map are expected to accurately reconstruct the input image. As mentioned in the previous section, the parameters β and ω are set to values significantly smaller than 1 to emphasize the importance of the dependency term in the optimization process.

To prevent the strong amplification of noise in images with very low brightness, the formulation of the G matrix is also modified as follows:

$$G = K \circ \nabla \hat{I} \tag{7}$$

$$K = 1 + \lambda e^{-|\nabla \hat{I}|/\sigma} \tag{8}$$

In which

$$\nabla \hat{I} = \begin{cases} 0, & if\ |\nabla I| < \varepsilon \\ \nabla I, & otherwise \end{cases} \tag{9}$$

Unlike the formulation in (4), small gradients (i.e., noise) are suppressed before amplification.

Both optimization problems (3) and (6) are non-convex due to the presence of the $R \circ L$ term. In Li's method, the alternating direction method (ADM) is used to solve this problem. Although ADM was originally proposed for convex optimization, recent studies have provided convergence guarantees for ADM in non-convex optimization problems [33,34]. In practice, we observe that this algorithm converges for all test images with reasonable regularization parameters.

The following presents the solution to problem (6). The solution to (3) can be obtained similarly. By replacing ∇L in the second term with an auxiliary variable T, the objective function (6) can be rewritten as follows:

$$\begin{aligned} \arg\min_{R,L,N,T} & \| R \circ L + N - I \|_F^2 + \beta \| T \|_1 + \delta \| N \|_F^2 \\ & + \omega \| \nabla R - G \|_F^2, \quad s.t. T = \nabla L \end{aligned} \tag{10}$$

By introducing a Lagrange coefficient Z to remove the equality constraint, we have the augmented Lagrange function (11)

$$\begin{aligned} L(R,L,N,T,Z) = & \| R \circ L + N - I \|_F^2 + \beta \| T \|_1 \\ & + \omega \| \nabla R - G \|_F^2 + \delta \| N \|_F^2 + \Phi(Z, \nabla L - T) \end{aligned} \tag{11}$$

Where $\Phi(A,B) = \langle A,B \rangle + \frac{u}{2} \| B \|_F^2$ and $\langle .,. \rangle$ denotes the inner matrix product. μ is a positive scalar. The equivalent objective function can be solved by iteratively updating each variable while keeping the other variables estimated in the previous iteration as constant. The solutions of the kth iteration of the sub-problems are presented below.

Sub-problem R:

Ignoring the statements unrelated to R, we have the following optimization problem:

$$\arg\min_R \| R \circ L^{(k)} + N^{(k)} - I \|_F^2 - \omega \| \nabla R - G \|_F^2 \tag{12}$$

We rewrite the first sentence in such a way that the problem becomes a classical least squares problem:

$$\arg\min_R \| \tilde{I}^{(k)} r + n^{(k)} - i \|_F^2 - \omega \| \nabla R - G \|_F^2 \tag{13}$$

Where I is the copied matrix L and $\tilde{I}$ denotes a diagonal matrix with I as its elements. The same notation is used for the other matrices (r, i, n, t, g and z corresponding to R, I, N, T, G and Z, respectively). Differentiating (13) with respect to R and setting the derivative equal to zero, we have the following equation:

$$\begin{aligned} & (\tilde{I}^{(k)})^T (\tilde{I}^{(k)} r + n^{(k)} - i) + 2\omega D^T (Dr - g) = 0 \\ & (f(\tilde{I}^{(k)}) + \omega f(D)) r = \tilde{I}^{(k)} (i - n^{(k)}) + \omega D^T g r^{(k+1)} \\ & = (f(\tilde{I}^{(k)}) + \omega f(D))^{-1} (\tilde{I}^{(k)} (i - n^{(k)}) + \omega D^T g) \end{aligned} \tag{14}$$

Where D is the discrete gradient operator.

Sub-problem L:

Collecting the sentences about L leads to the following problem:

$$\arg\min_L \| R^{(k+1)} \circ L + N^{(k)} - I \|_F^2 + \Phi(Z^{(k)}, \nabla L - T^{(k)}) \tag{15}$$

Similar to the previous derivation, the solution L is given as:

$$\begin{aligned} I^{(k+1)} = & \left(2 f(\tilde{r}^{(k+1)}) + \mu f(D) \right)^{-1} \\ & \times \left(2 \tilde{r}^{(k+1)} (i - n^{(k+1)}) + \mu D^T (t^{(k)} - \frac{z^{(k)}}{\mu}) \right) \end{aligned} \tag{16}$$

Sub-problem N:

By holding variables other than N constant, the problem becomes:

$$\arg\min_N \| R^{(k+1)} \circ L^{(k+1)} + N - I \|_F^2 + \delta \| N \|_F^2 \tag{17}$$

The closed-form solution to this quadratic problem is given as follows:

$$N^{(k+1)} = (I - R^{(k+1)} \circ L^{(k+1)}) / (1 + \delta) \tag{18}$$

In which the division is done element by element.

Sub-problem T:

Removing sentences without T leads to the following problem:

$$\arg\min_T \beta \| T \|_1 + \Phi(Z^{(k)}, \nabla L^{(k+1)} - T) \tag{19}$$

The solution (19) can be obtained by performing a contraction operation:

$$T^{(k+1)} = S_{\frac{\beta}{\mu^{(k)}}} \left(\nabla L^{(k+1)} + \frac{Z^{(k)}}{\mu^{(k)}} \right) \tag{20}$$

Where $S_\varepsilon(x) = sign(x)\max(|x|-\varepsilon,0)$, where the calculations are performed element-by-element.

Update Z and μ:

The auxiliary matrix Z and the penalty scalar μ are updated as follows:

$$Z^{(k+1)} = Z^{(k)} + \mu^{(k)}(\nabla L^{(k+1)} - T^{(k+1)}) \quad (21)$$
$$\mu^{(k+1)} = \mu^{(k)}\rho,\ \rho > 1$$

The entire iteration stops only if the difference between $R^{(k)}$ and $R^{(k+1)}$ or the difference between $L^{(k)}$ and $L^{(k+1)}$ is smaller than a threshold, e.g. 10^{-3} in practice, or if the maximum number of iterations has been reached.

2.2. Brightness Adjustment with PSO Optimization Algorithm

After estimating the luminance (L) and reflectance (R) components, the final step involves adjusting L to enhance the visibility of the input image. Gamma correction is employed for this brightness adjustment. The enhanced V channel image, denoted as Iˆ, is produced as follows:

$$\hat{I} = R \circ \hat{L} \quad (22)$$
$$\hat{L} = L^{\frac{1}{\gamma}}$$

Where γ is estimated using the PSO algorithm. It is important to note that the luminance does not require normalization prior to gamma correction, as the input V channel image is already normalized within the interval [0, 1]. Finally, the enhanced HSV image is converted back to the RGB color space, yielding the final enhanced image Ŝ.

After estimating the luminance (L) and reflectance (R) components, the final step involves adjusting the luminance (L) component using the PSO algorithm to determine the optimal value of the gamma parameter (γ). In this approach, the quality of the enhanced image is evaluated using a multi-part loss function, which the PSO algorithm aims to minimize.

The overall loss function is expressed as the sum of the entropy loss functions $(Loss_{Entropy})$, edge content $(Loss_{Edges})$, and the desired brightness mean $(Loss_{Mean})$:

$$Loss = W_1 Loss_{Entropy} + W_2 Loss_{Edges} + W_3 Loss_{Mean} \quad (23)$$

Where W_1, W_2, W_3 are the hyperparameters of the loss functions.

2.2.1. Entropy Loss Function ($Loss_{Entropy}$)

Entropy is a measurable property associated with randomness or uncertainty. In (25), P represents the probability of occurrence of each brightness level j [35].

$$Loss_{Entropy} = (\frac{E}{8} - 1)^2 \quad (24)$$

$$E = -\sum_{j=0}^{255} p(j) \times \log_2(p(j)) \quad (25)$$

2.2.2. Edge Content Loss Function ($Loss_{Edges}$)

$$Loss_{Edges} = (\frac{N_E}{N_T} - 0.5)^2 \quad (26)$$

Where N_E is the number of edge pixels detected by the Canny edge detection algorithm and N_T is the total number of pixels in the image.

2.2.3. Average Loss Function of Desired Brightness ($Loss_{Mean}$)

$$Loss_{Mean} = (ave_s - 0.6)^2 \quad (27)$$

Where ave_s is the average of the pixel values of the improved image (normalized to a range of 0 to 1).

2.2.4. Steps of the PSO Evolutionary Optimization Algorithm

1) Definition of search space and population initialization: A range for the gamma parameter is determined, and a population of particles with initial gamma values is created.

2) Evaluation of particle performance with multi-part loss function: For each particle (suggested gamma value):

The final improved image is generated using the gamma value of that particle

3) The overall loss function is calculated for the improved image.

4) Update local and global best: The local best performance (lowest loss) for each particle and the global best performance (lowest loss in the entire population) are updated.

5) Update particle velocity and position: The velocity and position of each particle are updated based on the local and global bests, using standard PSO equations.

6) Stopping criterion: The iterative process continues until a stopping criterion is met.

7) Selecting the best parameter: The gamma value corresponding to the best particle, which has the lowest loss function value at the end of the PSO process, is selected as the optimal gamma value for adjusting the brightness of the input image.

8) Using the multi-part loss function in the PSO algorithm, the gamma parameter adjustment process is guided such that a balance is established between increasing information (entropy),

preserving details (edges), and achieving the desired brightness (light) in the improved image.

3. Comparison and Evaluation

To evaluate the performance of the proposed method, its results were compared with those of several state-of-the-art low-light image enhancement techniques. LDR [36] is a traditional method for image contrast enhancement that operates by analyzing 2D histograms and enhancing the gray level differences between adjacent pixels in a layered structure. LIME [14] is a light map estimation-based method that aims to improve the brightness and contrast of low-light images by estimating and adjusting an optimized light map. KinD [37] is a deep learning-based method inspired by Retinex theory, which decomposes images into luminance and reflectance components and enhances them separately. Li [17] is a robust Retinex model-based method that improves low-light images by preserving structure and reducing noise, taking the noise term into account. IceNet [38] is a convolutional neural network (CNN)-based method that allows users to interactively adjust image contrast. IceNet can also automatically enhance images. LLFormer [5] is a transformer architecture-based method specifically designed for enhancing high-resolution low-light images and employs automatic attention mechanisms to extract image features. Zero-DiDCE [7] is a novel and optimized deep learning-based method that builds upon the previous version of Zero-DCE. By applying an improved architecture and training objectives, it delivers better performance in enhancing low-light images without requiring paired training data. This method is recognized as one of the leading and most powerful approaches in the field of low-light image enhancement without reference.

3.1. Dataset

MEF and HDR methods [39] can produce images of significantly higher quality compared to a single ordinary photograph. These methods utilize the combination of multiple images of a fixed scene to generate a single image with enhanced quality and resolution. These techniques have been used to create the reference images in the SICE dataset [40]. The SICE dataset consists of sequences of images captured at different exposure levels along with their corresponding reference images. It contains over 4,000 images in total, including 589 sequences of scenes with varying exposures and their respective reference images. The dataset is divided into two parts: the first part contains 360 image sequences, and the second part contains 229 sequences. Figure 2 shows a sequence of images of a fixed scene from the SICE dataset alongside its corresponding reference image. Figure 3 displays examples illustrating the diversity of images within this dataset.

.

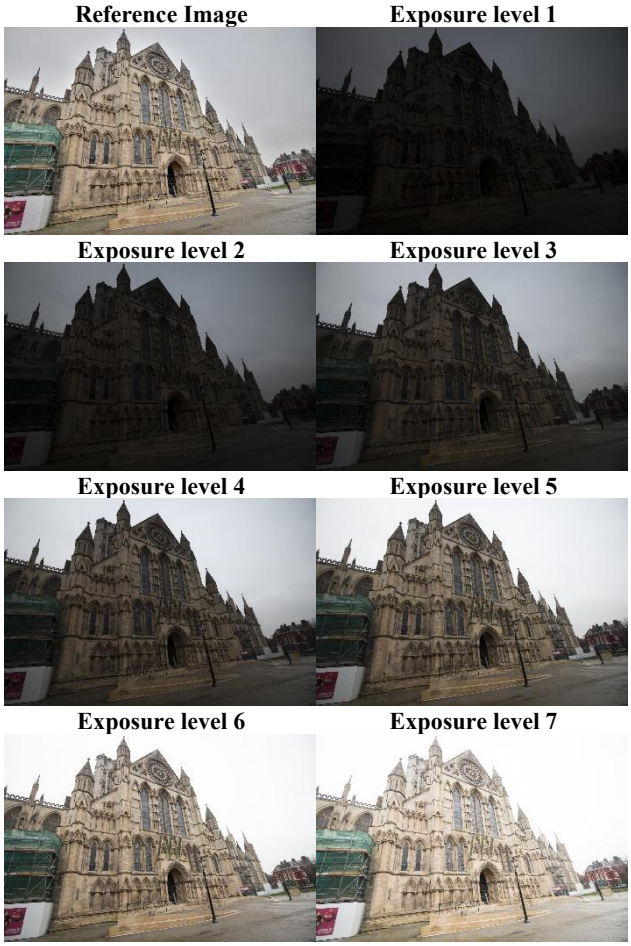

Figure 2. An example of a sequence of images with different exposures from the SICE dataset.

The selection of this dataset is guided by two primary objectives. First, the dataset should include sufficiently long sequences of images with varying exposures that cover diverse scenes. These scenes encompass indoor environments with artificial lighting as well as outdoor settings under natural sunlight. Additionally, the number of sequences and the diversity of their exposures must be adequate. Second, each sequence should have a high-quality reference image available, which can be used to compute scores for metrics that require a reference image.

Figure 3. shows images of different scenes from the SICE dataset [34].

3.2. Implementation Details

The method for combining and proportionally weighting each loss function is presented in Table 1. Due to differences in the magnitudes of each loss function, appropriate hyperparameters were introduced into the formula for each loss term. The overall loss function is defined as the sum of three individual loss functions, with the aim of equalizing the impact of each loss within the total loss. During a testing phase on various images from the dataset, the average output values of each loss function were calculated without applying hyperparameters. It was observed that the mean output values of the loss functions varied and spanned different ranges. To normalize the influence of each loss function in the total loss, the corresponding hyperparameters were calculated based on the average outputs, ensuring that the contributions of each loss function are balanced. The values of these hyperparameters, along with the average outputs of each loss function, are provided in Table 1.

Table 1. Loss functions hyperparameter and value.

Loss function	hyperparameter	Loss average	Loss range [min-max]
$Loss_{Ent}$	$W_{Ent} = 0.961$	0.520	[0-1]
$Loss_{Edges}$	$W_{Edges} = 2.659$	0.188	[0-1]
$Loss_{Mean}$	$W_{Mean} = 1.436$	0.348	[0-1]

For the PSO algorithm, the population size and the number of iterations were set to 200 and 50, respectively. These values were chosen because they yielded optimal results; increasing these parameters did not further improve the outcome but only increased the algorithm's processing time and computational cost. The gamma parameter range was set to [0, 5]. The minimum gamma value was set to 0, as negative values are not permissible. The maximum gamma value was set to 5, as values exceeding this threshold tend to excessively darken the image.

3.3. Quantitative Comparison

To conduct a quantitative comparison, several benchmark and reference image quality evaluation metrics were employed on the SICE dataset. These metrics included PSNR, SSIM, PIQE, NIQE, BRISQUE, and NIMA, and were applied to the enhanced images generated by each method. A subset of 100 low-light images was selected from the SICE dataset. The results of the quantitative comparison on the SICE dataset are presented in Table 2. As shown in this table, the proposed method demonstrates competitive or superior performance compared to the other methods across several metrics. Notably, the proposed method achieves the highest score in structure preservation, as indicated by the SSIM metric. It also yields promising results in benchmark quality evaluations, as shown by the PIQE, NIQE, and BRISQUE metrics, suggesting the generation of images with reduced distortion and enhanced naturalness.

Furthermore, the NIMA scores indicate that the images enhanced by the proposed method also achieve the highest aesthetic quality ratings. In terms of the PSNR metric, deep learning-based methods such as KinD and LIME often exhibit superior performance, likely due to their direct learning of mappings from low-light images to normal-light images and their capacity to model complex data dependencies.

The Zero-DiDCE and LLFormer methods also demonstrate highly competitive performance. The Li method, as a model-based approach relying on light map estimation, provides acceptable results. IceNet, with its emphasis on user interaction, may

exhibit different performance characteristics in automated comparisons. Finally, the LDR method, as a traditional technique, generally performs less effectively compared to deep learning methods that utilize more complex models.

For a more precise comparison between the proposed method and conventional approaches, the score of each evaluation metric is normalized to the range [0, 1] using the minimum and maximum values of the metric's evaluation range. Then, the average normalized scores obtained by each method are calculated. According to Equation 28, score represents the obtained score, while max and min denote the maximum and minimum values of the evaluation range for each metric, respectively. For metrics where a lower score indicates better performance, the normalized score is computed as $Norm = 1 - Norm$. The normalized scores for the metrics listed in Table 2 are presented in Table 3.

$$Norm = \frac{Score - Min}{Max - Min} \tag{28}$$

According to Table 3, the proposed method achieves the best scores in the SSIM, NIQE, and NIMA metrics. The LLFormer method attains the highest scores in the PIQE, BRISQUE, and DISTS metrics, while the KinD method performs best in the PSNR metric. In terms of average normalized scores, the proposed method ranks first overall. Each metric evaluates image quality from a different perspective, and a high score in a single metric does not necessarily indicate superior overall image quality. An image that achieves relatively good scores across most metrics generally exhibits higher quality. Therefore, a higher average score across multiple metrics reflects better overall image quality. Based on the average metric scores presented in Table 3, the proposed method is ranked first, followed by LLFormer and KinD in second and third places, respectively.

Table 2. Comparison of the evaluation metrics of low-light images enhanced by the proposed method with some other existing methods

	LDR [36]	LIME [14]	Li[17]	KinD[37]	IceNet [38]	LLFormer [5]	Zero-DiDCE[7]	Proposed method
PSNR↑	13.2	20.25	13.78	**21**	8.65	18.78	18.22	18.47
SSIM↑	0.49	0.79	0.67	0.73	0.29	0.76	0.76	**0.79**
NIQE↓	4.14	3.50	3.77	3.20	3.36	3.24	3.59	**3.02**
PIQE↓	56.25	55.36	54.64	48.09	44.01	**33.20**	45.00	40.80
Brisque↓	45.92	38.07	44.35	29.94	34.74	**25.58**	36.19	30.56
NIMA↑	4.92	5.35	4.07	5.00	5.22	4.41	5.42	**5.93**
DISTS↓	0.22	0.19	0.21	0.15	0.29	**0.14**	0.17	0.17
Run time↓ (ms)	49	245	873	8	**2**	68	15	962

Table 3. Average normalized scores of enhanced low-light images achieved by each method.

	LDR[36]	LIME[14]	Li[17]	KinD[37]	IceNet[38]	LLFormer [5]	Zero-DiDCE [7]	Proposed method
PSNRnorm↑	0.17	0.25	0.17	**0.26**	0.11	0.23	0.23	0.23
SSIMnorm↑	0.50	0.79	0.68	0.73	0.30	0.76	0.77	**0.80**
NIQEnorm↑	0.59	0.65	0.62	0.68	0.66	0.68	0.64	**0.70**
PIQEnorm↑	0.44	0.45	0.45	0.52	0.56	**0.67**	0.55	0.59
Brisquenorm↑	0.54	0.62	0.56	0.70	0.65	**0.74**	0.64	0.69
NIMAnorm↑	0.44	0.48	0.34	0.45	0.47	0.38	0.49	**0.55**
DISTSnorm↑	0.78	0.81	0.79	0.85	0.71	**0.86**	0.83	0.83
Average↑	0.49	0.58	0.52	0.60	0.49	0.62	0.59	**0.63**
Rank↓	8	5	6	3	7	2	4	**1**

3.4. Qualitative Comparison

In addition to the quantitative evaluations, qualitative (visual) comparisons of the results obtained by the proposed method and the compared methods are presented in Figures 4 and 5. These visual analyses indicate that the proposed method effectively improves visibility, enhances contrast, and preserves details in dark regions, while simultaneously suppressing artifacts and noise. In comparison to certain deep learning-based methods, our approach, grounded in a robust and optimized Retinex model, in some instances yields more natural-looking results with superior structure preservation and avoids the generation of unnatural colors occasionally observed in deep learning techniques.

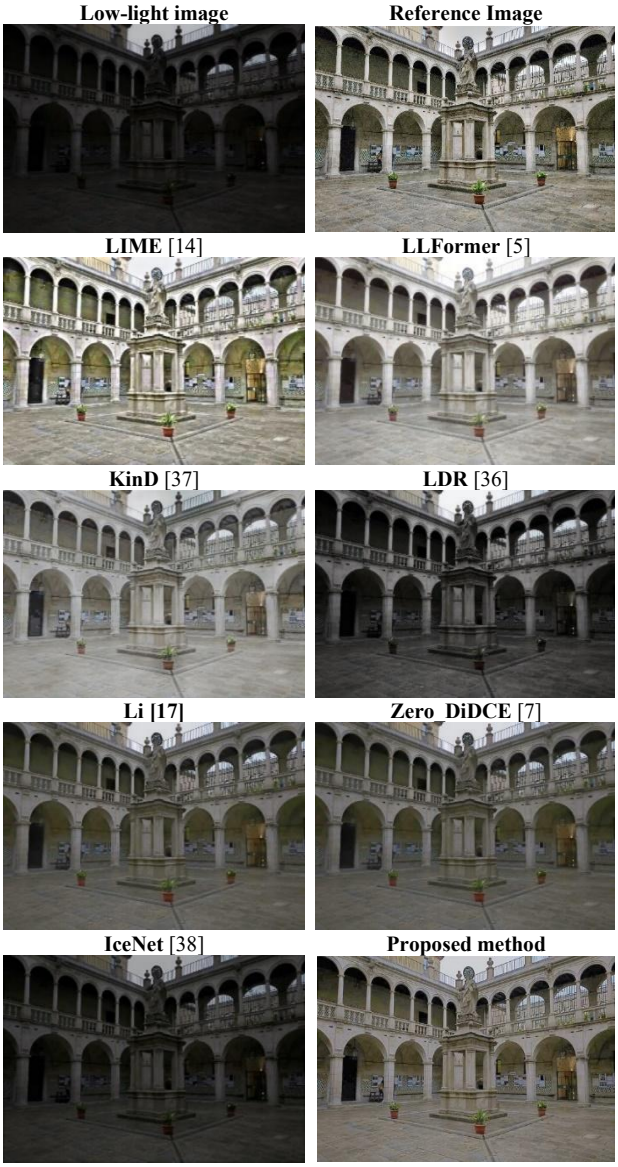

Figure 4. The performance comparison of proposed and existing methods using the low-light image (SICE dataset).

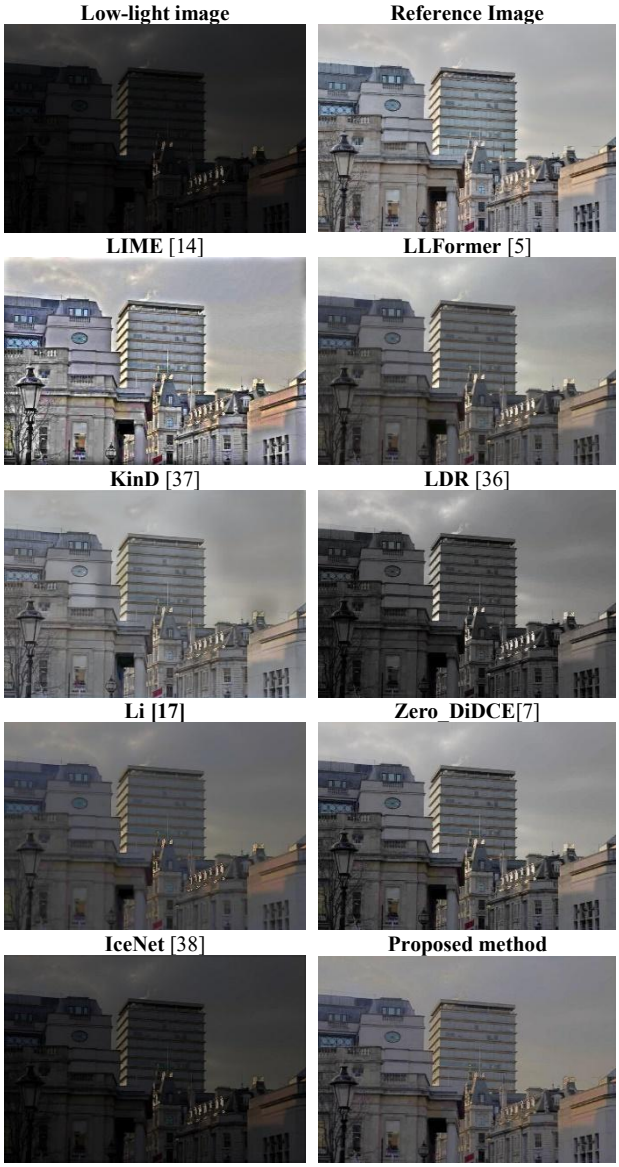

Figure 5. The performance comparison of proposed and existing methods using the low-light image (SICE dataset).

The novel Zero-DiDCE method also demonstrates substantial visual improvements. The Li and LIME methods also provide significant enhancements in visibility. IceNet can produce favorable results under user interaction. The LDR method, while potentially increasing overall contrast, may lead to a loss of fine details and is not as effective in noise reduction. KinD and LLFormer also exhibit considerable visual improvements.

3.5. Discussion

Structure and detail preservation: The proposed method effectively preserves the original image structure and enhances the visibility of details in dark regions, as evidenced by the SSIM scores and visual comparisons. This highlights the method's capability to improve image quality without introducing significant structural distortions.

Natural visual quality: The non-reference image quality assessment metrics (PIQE, NIQE, and BRISQUE) indicate that the enhanced images achieve acceptable quality in terms of human perception and naturalness. This suggests that the proposed approach produces visually pleasing results without introducing significant artifacts.

Flexibility in noise handling: By incorporating noise terms into the robust Retinex model, the proposed method demonstrates improved adaptability in handling various types of noise present in low-light images. This contrasts with methods that assume specific noise models or lack explicit noise consideration.

No requirement for paired training data: Unlike many deep learning-based methods, including state-of-the-art approaches such as KinD, Rethinking Zero-DCE, and LLFormer, the proposed method does not require large paired

training datasets. Furthermore, compared to light map estimation-based methods like LIME and Li's Retinex-based method, our approach can yield superior results in certain scenarios by explicitly considering noise and leveraging PSO optimization. IceNet's optimal performance also depends on user interaction, which is not a requirement for our method.

Benchmark performance (PSNR): In terms of the PSNR metric, the proposed method may exhibit inferior performance compared to some advanced deep learning-based methods, including KinD, Rethinking Zero-DCE, and LLFormer. This potential discrepancy can be attributed to our method's emphasis on preserving image structure and producing more natural visual outputs, rather than strictly reconstructing the reference image on a pixel-by-pixel basis. Similarly, light map estimation-based methods such as LIME and Li's Retinex-based method may also achieve higher PSNR scores in some cases. The LDR method generally performs poorly on pixel-accuracy-based metrics like PSNR, and IceNet's performance in automated comparisons may be limited due to its interactive nature.

Computational complexity: The iterative optimization process inherent in the PSO algorithm can be computationally demanding and may require more processing time compared to some direct methods or deep learning-based methods (once trained). Light map estimation-based methods like LIME are typically less computationally intensive, while optimization-based methods such as Li's can also incur significant processing time. The LDR method generally exhibits lower computational complexity, and deep learning-based methods like KinD and Rethinking Zero-DCE can achieve high processing speeds after the training phase. The transformer architecture employed by LLFormer can lead to substantial computational overhead. IceNet's computational complexity depends on the architecture of the underlying network.

4. Conclusion

In this paper, we present a novel method for enhancing images captured under low-light conditions. This method utilizes a robust Retinex model combined with a PSO-based optimization approach. A key contribution of the proposed method is the incorporation of a noise term within the Retinex model, enabling improved handling of noise inherent in low-light images. Furthermore, the use of the PSO evolutionary optimization algorithm, guided by a multi-part loss function, facilitates the automatic and effective adjustment of the gamma parameter, leading to enhanced final results.

The results of quantitative and qualitative comparisons performed on the SICE dataset demonstrate that our proposed method achieves performance comparable to or exceeding that of several state-of-the-art methods. This includes preserving image structure, generating natural-looking images, and suppressing noise. The method's performance is competitive with powerful deep learning-based methods such as KinD, Zero-DiDCE, and LLFormer, Retinex-based methods like Li's, and luminance map estimation-based methods, while surpassing the performance of the traditional LDR method. In contrast to IceNet, our method offers a fully automated approach. While deep learning-based methods may excel in certain pixel-difference-based metrics like PSNR, our method demonstrates competitiveness in producing images with desirable visual quality and preserving structural details. Additionally, it offers advantages in terms of not requiring paired training data and its foundation in a physical model-based framework. The strong competition with state-of-the-art and highly efficient methods, coupled with acceptable performance compared to other approaches, underscores the potential of our proposed method. Future work could explore further optimization of the PSO algorithm to reduce computational complexity and enhance processing speed. Additionally, research into automated techniques for tuning model parameters (such as β and ω) and PSO loss function weights could prove beneficial. Extending this method for low-light video enhancement presents another promising research direction. Finally, investigating the method's performance across diverse types of low-light images and in various practical applications would contribute to a more comprehensive understanding of its capabilities and facilitate a more accurate comparison with emerging methods.

References

[1] M. A. Al Wadud, M. H. Kabir, M. A. A. Dewan, and O. Chae, "A dynamic histogram equalization for image contrast enhancement," *IEEE transactions on consumer electronics*, Vol. *53*, pp. 593-600, 2007.

[2] H. Rastegar, H. Khotanlou, "Image Dehazing Using a Convolutional Autoencoder Network with Integrated Convolutional Block Attention," *Journal of AI and Data Mining,* Vol. 13, pp. 393-405, 2025.

[3] K. Dabov, A. Foi, V. Katkovnik, and K. Egiazarian, "Image denoising by sparse 3-D transform-domain collaborative filtering," *IEEE Transactions on Image Processing,* Vol. 16, pp. 2080-2095, 2007.

[4] K. G. Lore, A. Akintayo, and S. Sarkar, "LLNet: A deep autoencoder approach to natural low-light image enhancement," *Pattern Recognition*, Vol. 61, pp. 650-662, 2017.

[5] T. Wang, K. Zhang, T. Shen, W. Luo, B. Stenger, and T. Lu, "Ultra-High-Definition Low-Light Image Enhancement: A Benchmark and Transformer-Based Method," in *Proceedings of the 37th AAAI Conference on Artificial Intelligence,* 2023, pp. 2654-2662.

[6] C. Guo *et al.*, "Zero-reference deep curve estimation for low-light image enhancement," in *Proceedings of the IEEE Computer Society Conference on Computer Vision and Pattern Recognition*, 2020, pp. 1780-1789.

[7] A. Mi, W. Luo, Y. Qiao, and Z. Huo, "Rethinking Zero-DCE for Low-Light Image Enhancement," *Neural Processing Letters,* Vol. 56.2, pp. 93, 2024.

[8] X. Gao, K. Zhao, L. Han, and J. Luo, "BézierCE: Low-Light Image Enhancement via Zero-Reference Bézier Curve Estimation," *Sensors*, Vol. 23.23, pp. 9593, 2023.

[9] E. H. Land, "The retinex theory of color vision," *Scientific american*, Vol. 237.6, pp. 108-129, 1977.

[10] D. J. Jobson, Z. U. Rahman, and G. A. Woodell, "Properties and performance of a center/surround retinex," *IEEE transactions on image processing,* Vol. 6.3, pp. 451-462, 1997.

[11] D. J. Jobson, Z. U. Rahman, and G. A. Woodell, "A multiscale retinex for bridging the gap between color images and the human observation of scenes," *IEEE transactions on image processing,* Vol. 6.7, pp. 965-976, 1997.

[12] S. Wang, J. Zheng, H. M. Hu, and B. Li, "Naturalness preserved enhancement algorithm for non-uniform illumination images," *IEEE transactions on image processing,* Vol. 22.9, pp. 3538-3548, 2013.

[13] X. Fu, D. Zeng, Y. Huang, Y. Liao, X. Ding, and J. Paisley, "A fusion-based enhancing method for weakly illuminated images," *Signal Processing*, Vol. 129, pp. 82-96, 2016.

[14] X. Guo, Y. Li, and H. Ling, "LIME: Low-light image enhancement via illumination map estimation," *IEEE transactions on image processing,* Vol. 26.2, pp. 982-993, 2016.

[15] X. Fu, D. Zeng, Y. Huang, X. P. Zhang, and X. Ding, "A Weighted Variational Model for Simultaneous Reflectance and Illumination Estimation," in *Proceedings of the IEEE Computer Society Conference on Computer Vision and Pattern Recognition*, 2016, pp. 2782-2790.

[16] J. Hai *et al.*, "R2RNet: Low-light image enhancement via Real-low to Real-normal Network," *Journal of Visual Communication and Image Representation*, Vol. 90, pp. 103712, 2023.

[17] M. Li, J. Liu, W. Yang, X. Sun, and Z. Guo, "Structure-Revealing Low-Light Image Enhancement Via Robust Retinex Model," *IEEE transactions on image processing,* Vol. 27.6, pp. 2828-2841, 2018.

[18] E. Provenzi, D. Marini, L. De Carli, and A. Rizzi, "Mathematical definition and analysis of the Retinex algorithm," *Journal of the Optical Society of America A*, Vol. 22.12, pp. 2613-2621, 2005.

[19] R. Grosse, M. K. Johnson, E. H. Adelson, and W. T. Freeman, "Ground truth dataset and baseline evaluations for intrinsic image algorithms," in *Proceedings of the IEEE International Conference on Computer Vision*, 2009, pp. 2335-2342.

[20] Q. Chen and V. Koltun, "A simple model for intrinsic image decomposition with depth cues," in *Proceedings of the IEEE International Conference on Computer Vision*, 2013, pp. 241-248.

[21] P. Y. Laffont, A. Bousseau, and G. Drettakis, "Rich intrinsic image decomposition of outdoor scenes from multiple views," *IEEE transactions on visualization and computer graphics*, Vol. 19.2, pp. 210-224, 2012.

[22] S. Bell, K. Bala, and N. Snavely, "Intrinsic images in the wild," *ACM Transactions on Graphics*, Vol. 33.4, pp. 1-12, 2014.

[23] A. Meka, M. Zollhöfer, C. Richardt, and C. Theobalt, "Live intrinsic video," *ACM Transactions on Graphics*, Vol. 35.4, pp. 1-14, 2016.

[24] J. T. Barron and J. Malik, "Color constancy, intrinsic images, and shape estimation," in *European Conference on Computer Vision*. Berlin, Heidelberg, 2012, pp. 57-70.

[25] Y. Li and M. S. Brown, "Single image layer separation using relative smoothness," in *Proceedings of the IEEE conference on computer vision and pattern recognition*, 2014, pp. 2752-2759.

[26] M. Elad, "Retinex by two bilateral filters," in *International conference on scale-space theories in computer vision*. Berlin, Heidelberg, 2005, pp. 217-229.

[27] W. Li, B. Gu, J. Huang, and M. Wang, "Novel Retinex algorithm by interpolation and adaptive noise suppression," *Journal of Central South University*, Vol. 19.9, pp. 2541-2547, 2012.

[28] X. Yu, X. Luo, G. Lyu, and S. Luo, "A novel Retinex based enhancement algorithm considering noise," in *IEEE/ACIS 16th International Conference on Computer and Information Science (ICIS)*, 2017, pp. 649-654.

[29] Z. Farbman, R. Fattal, D. Lischinski, and R. Szeliski, "Edge-preserving decompositions for multi-scale tone and detail manipulation," *ACM transactions on graphics (TOG)*, Vol. 27.3, pp. 1-10, 2008.

[30] X. Guo, Y. Li, J. Ma, and H. Ling, "Mutually Guided Image Filtering," *25th ACM international conference on Multimedia*, 2017, pp. 1283-1290.

[31] X. Fu, Y. Liao, D. Zeng, Y. Huang, X. P. Zhang, and X. Ding, "A Probabilistic Method for Image

Enhancement with Simultaneous Illumination and Reflectance Estimation," *IEEE Transactions on Image Processing*, Vol. 24.12, pp. 4965-4977, 2015.

[32] C. Wang and Z. F. Ye, "Variational enhancement for infrared images," *Journal of Infrared and Millimeter Waves*, Vol. 25.4, pp. 306-310, 2006.

[33] Y. Wang, W. Yin, and J. Zeng, "Global Convergence of ADMM in Nonconvex Nonsmooth Optimization," *Journal of Scientific Computing*, Vol. 78.1, pp. 29-63, 2019.

[34] Y. Xu, W. Yin, Z. Wen, and Y. Zhang, "An alternating direction algorithm for matrix completion with nonnegative factors," *Frontiers of Mathematics in China*, Vol. 7.2, pp. 365-384, 2012.

[35] Y. Zhou, C. Shi, B. Lai, and G. Jimenez, "Contrast enhancement of medical images using a new version of the World Cup Optimization algorithm," *Quantitative imaging in medicine and surgery*, Vol. 9.9, pp. 1528, 2019.

[36] C. Lee, C. S. Kim, and C. Lee, "Contrast enhancement based on layered difference representation of 2D histograms," *IEEE transactions on image processing*, Vol. 22.12, pp. 5372-5384, 2013.

[37] Y. Zhang, J. Zhang, and X. Guo, "Kindling the darkness: A practical low-light image enhancer," in *Proceedings of the 27th ACM international conference on multimedia*, 2019, pp. 1632-1640.

[38] K. Ko and C. S. Kim, "IceNet for Interactive Contrast Enhancement," *IEEE Access*, Vol. 9, pp. 168342-168354, 2021.

[39] C. Schlick, "Quantization Techniques for Visualization of High Dynamic Range Pictures," in *Photorealistic rendering techniques*. Berlin, Heidelberg, 1995, pp. 7-20.

[40] J. Cai, S. Gu, and L. Zhang, "Learning a deep single image contrast enhancer from multi-exposure images," *IEEE Transactions on Image Processing*, Vol. 27.4, pp. 2049-2062, 2018.

بهبود روشنایی تصاویر کم نور مبتنی بر نظریه رتینکس به کمک الگوریتم تکاملی PSO

علی شعبانی بدیع[۱]، کامبیز رهبر[۱،*] ، ضیاالدین بهشتی فرد[۱] و مریم خادمی[۲]

[۱] گروه مهندسی کامپیوتر، واحد تهران جنوب، دانشگاه آزاد اسلامی، تهران، ایران.

[۲] گروه ریاضی، واحد تهران جنوب، دانشگاه آزاد اسلامی، تهران، ایران.

ارسال ۲۰۲۵/۰۶/۰۱؛ بازنگری ۲۰۲۵/۰۸/۱۵؛ پذیرش ۲۰۲۵/۱۰/۱۴

چکیده:

این مقاله یک رویکرد جدید برای بهبود کیفیت تصاویر اخذ شده در شرایط کم نور معرفی می‌کند. این روش با استفاده از الگوریتم بهینه‌سازی ازدحام ذرات (PSO) پارامترهای روش شناخته شده Li را بهینه سازی می‌کند. سهم کلیدی این تحقیق، فرمول‌بندی یک تابع زیان جامع برای الگوریتم PSO است که از ادغام توابع زیان آنتروپی، پیکسلهای لبه و متوسط روشنایی مطلوب تصویر به دست آمده است. هدف از فرآیند بهینه‌سازی، تعیین مجموعه پارامترهای بهینه برای روش پایه به منظور حفظ ساختار تصویر، بهبود روشنایی با حفظ جزئیات لبه ها، و تنظیم نور کلی تصویر در محدوده مطلوب می باشد. تابع زیان آنتروپی جزئیات تصویر را افزایش می‌دهد که منجر به بهبود کنتراست تصویر می‌شود. عملکرد تابع زیان لبه، لبه ها و نقاط مرزی تصویر را افزایش می‌دهد. افزایش پیکسل‌های لبه خطوط مرزی اشیاء موجود در تصویر را تقویت می‌کند، که در نتیجه وضوح تصویر را بهبود می‌بخشد. عملکرد تابع زیان روشنایی، نور تصویر را در حالت مطلوب تنظیم می‌کند. میانگین روشنایی پیکسل‌های تصویر به مقدار ۰٫۶ (نرمال سازی شده در محدوده صفر تا یک) نزدیک می‌شود که به تنظیم روشنایی مطلوب تصویر کمک می‌کند. از یک استراتژی بهینه‌سازی تکراری برای تنظیم پارامترهای روش پایه استفاده شده است. عملکرد روش پیشنهادی از طریق تحلیل‌های کمی و کیفی بر روی مجموعه داده SICE مورد ارزیابی قرار گرفته و با چند روش پیشرفته بهبود تصاویر کم نور مقایسه شده است. ارزیابی کمی، با استفاده از معیارهایی مانند PSNR، SSIM، PIQE، NIQE، BRISQUE و NIMA، نشان می‌دهد که تنظیم پارامترهای روش پایه، با استفاده از الگوریتم PSO و تابع زیان جامع ما، منجر به عملکرد رقابتی یا برتر در حفظ ساختار و جزئیات تصویر، تولید تصاویر با کیفیت بصری طبیعی و سرکوب نویز در مقایسه با بسیاری از روش‌های موجود می‌گردد. این رویکرد کارایی الگوریتم تکاملی PSO در یافتن تنظیمات بهینه برای یک روش مبتنی بر مدل فیزیکی را با هدف بهبود کیفیت تصاویر کم نور به نمایش می‌گذارد.

کلمات کلیدی: بهبود تصاویر کم نور، الگوریتم تکاملی PSO ، نظریه رتینکس، اصلاح گاما.